JOURNAL OF THE MECHANICAL BEHAVIOR OF BIOMEDICAL MATERIALS 34 (2014) 349–357

Available online at www.sciencedirect.com

ScienceDirect

www.elsevier.com/locate/jmbbm

Research Paper

The effect of transient conditions on synovial fluid protein aggregation lubrication

*Connor William Myant**, *Philippa Cann*

Tribology Group, Imperial College London, London SW7 2AZ, UK

ARTICLE INFO

Article history:
Received 24 October 2013
Received in revised form
22 January 2014
Accepted 2 February 2014
Available online 7 February 2014

Keywords:
Metal-on-metal hips
Artificial joints
Film thickness
Wear
Bovine serum
Synovial fluid

ABSTRACT

Little is known about the prevailing lubrication mechanisms in artificial articular joints and the way in which these mechanisms determine implant performance. The authors propose that interfacial film formation is determined by rheological changes local to the contact and is driven by aggregation of synovial fluid proteins within the contact inlet region. A direct relationship between contact film thickness and size of the protein aggregation within the inlet region has been observed.

In this paper the latest experimental observations of the protein aggregation mechanism are presented for conditions which more closely mimic joint kinematics and loading. Lubricant films were measured for a series of bovine calf serum solutions for CoCrMo femoral component sliding against a glass disc. An optical interferometric apparatus was employed to study the effects of transient motion on lubricant film formation. Central film thickness was measured as a function of time for a series of transient entrainment conditions; start-up motion, steady-state and non-steady-state uni-directional sliding, and bi-directional sliding. The size of the inlet aggregations was found to be dependent upon the type of transient condition. Thick protective protein films were observed to build up within the main contact region for all uni-directional tests. In contrast the inlet aggregation was not observed for bi-directional tests. Contact film thickness and wear was found to be directly proportional to the presence of the inlet protein phase. The inlet phase and contact films were found to be fragile when disrupted by surface scratches or subjected to reversal of the sliding direction.

1. Introduction

Articular joint lubrication is one of the most difficult problems in tribology as these implants experience transient loading and kinematics and has a complex biphasic lubricating fluid (Dowson and Neville, 2006). As yet little is known about the prevailing lubrication mechanisms in artificial joints and this presents a potentially serious gap in our knowledge, as these mechanisms determine film formation and hence wear. There is currently a widespread tendency within the literature to confine the tribological mechanisms operating during the gait cycle to a single lubrication regime

*Corresponding author.
E-mail address: connor.myant@imperial.ac.uk (C.W. Myant).

http://dx.doi.org/10.1016/j.jmbbm.2014.02.005
1751-6161

Nomenclature

AA	adduction/abduction
BCS	bovine calf serum
CrCoMo	FS75 chromium, cobalt and molybdenum alloy
CoC	ceramic-on-ceramic
EHL	elastohydrodynamic lubrication
FE	flexion/extension
IOR	inward/outward rotation
LHMoM	large head metal-on-metal
MoM	metal-on-metal
MoP	metal-on-polymer
η	dynamic viscosity
OA	osteoarthritis
PAL	protein aggregation lubrication
R'	reduced radius
s	inlet reservoir length
SAPL	surface active phospholipid
SF	synovial fluid
R_a	arithmetic mean surface roughness
U	entrainment speed
W	applied load

(Smith et al., 2001). The two most popular theories are Boundary and Elasto-Hydrodynamic lubrication which differ significantly in film formation mechanisms, wear characteristics and the response to changing contact conditions (Myant and Cann, 2014). The arguments for (or against) these commonly held ideas were found to be overly simplistic; either ignoring the transient kinematic and loading conditions prevalent in artificial articular joints or the complex rheological and chemical nature of synovial fluid. Classical EHL models are commonly employed to predict film thickness, and hence performance, in artificial hips (Yew et al., 2004). This analysis is based on the flawed assumption that implant lubrication can be described by EHL mechanisms developed for simple Newtonian fluids in steady state conditions (Hamrock and Dowson, 1978).

Recently the authors have suggested a novel lubrication mechanism describing film formation for complex fluids containing proteins (Fan et al., 2011; Myant et al., 2012; Myant and Cann, 2013). The model has been developed entirely from experimental studies of model SF lubrication. One of the key findings is that the lubricant film thickness does not obey EHL rules; i.e. positive speed and negligible load dependency (Myant and Cann, 2014; Stachowiak and Batchelor, 2005). It was concluded that film thickness predictions could not be made using simple Newtonian fluid rheology and steady state contact conditions. Rather, in this model interfacial film formation is determined by rheological changes local to the contact and is driven by aggregation of proteins within the contact inlet region. This concentration of proteins now feeds the contact which a new lubricant phase; which has a greatly increased protein content and viscosity, causing much higher than predicted film thickness (Myant et al., 2012).

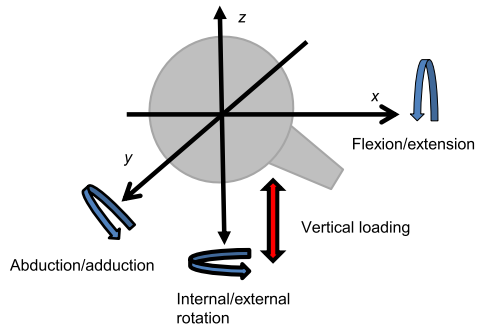

Fig. 1 – Representation of a hip joint showing all three axis of rotation.

Previous results demonstrated a clear correlation between inlet size and contact film thickness (Myant and Cann, 2013). Much of this earlier work studied simple uni-directional sliding contacts; however articular joints actually experience sliding on multiple axes and reversals in the sliding direction. It is likely that this gait like motion will disrupt the proteinacous inlet phase having a significant effect on contact film thickness. The introduction of wear debris or surface scratch may also disrupt lubricant film formation. This paper investigates the effect of inlet disruption on contact film thickness, caused by transient motion and the passage of surface scratches.

1.1. *Background*

Earlier results demonstrated that model SF solutions demonstrate complex time-dependent film thickness behaviour that is not characteristic of a simple Newtonian fluid (Fan et al., 2011). The effect of the deceasing gap height in the inlet region and relative motion of the surfaces (SRR) is to collect proteins at the entry to the contact. These conditions cause a protein enriched phase to form a new inlet reservoir. This process has been observed for similar complex fluids; and is termed bulk phase separation (Stokes et al., 2001). The new protein-gel phase has a much higher viscosity than the bulk solution. Consequently, a significantly thicker film is formed than would be predicted by classical EHL theory, when the bulk rheological properties are employed (Myant and Cann, 2013). The subsequent contact film thickness is controlled by the rheological properties of this new inlet reservoir and not the bulk solution. Contact entry of this protein phase is complex and dependent on operating conditions (speed, load, geometry) and lubricant properties (molecule size, concentration) (Myant et al., 2012). A direct relationship between contact film thickness and the length, and width, of protein aggregation within the inlet region has been observed (Myant and Cann, 2013). Thus we adopted the 'PAL—Protein Aggregation Lubrication' acronym identifying this process.

Our initial work was applied to simple pure sliding unidirectional contacts, which enabled us to determine the fundamental lubrication mechanisms occurring for protein containing fluids. However, in reality an articular joint undergoes complex kinematic and transient loading cycles.

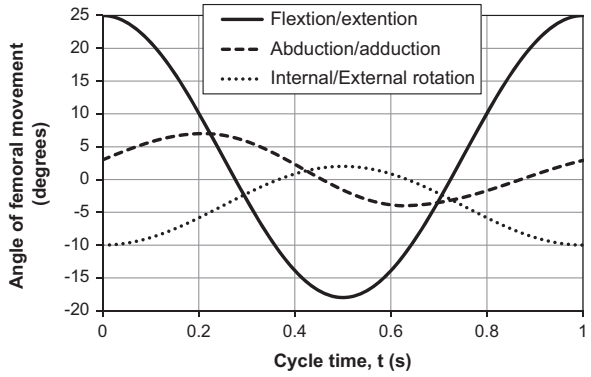

Fig. 2 – ISO standard #14242-1 hip gait cycle; angles of rotation around all three axis of rotation.

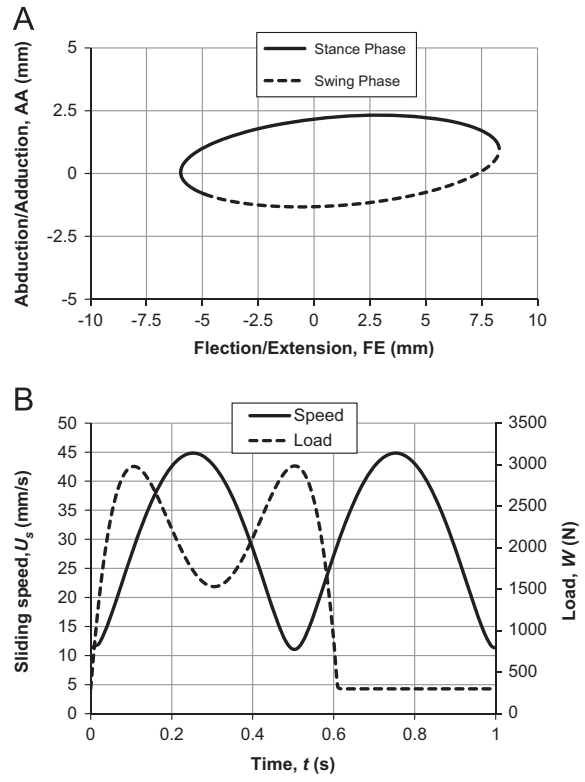

Fig. 3 – ISO standard #14242-1 hip gait cycle; (a) contact track for a 38 mm diameter femoral head, (b) speed and load for a single gait cycle.

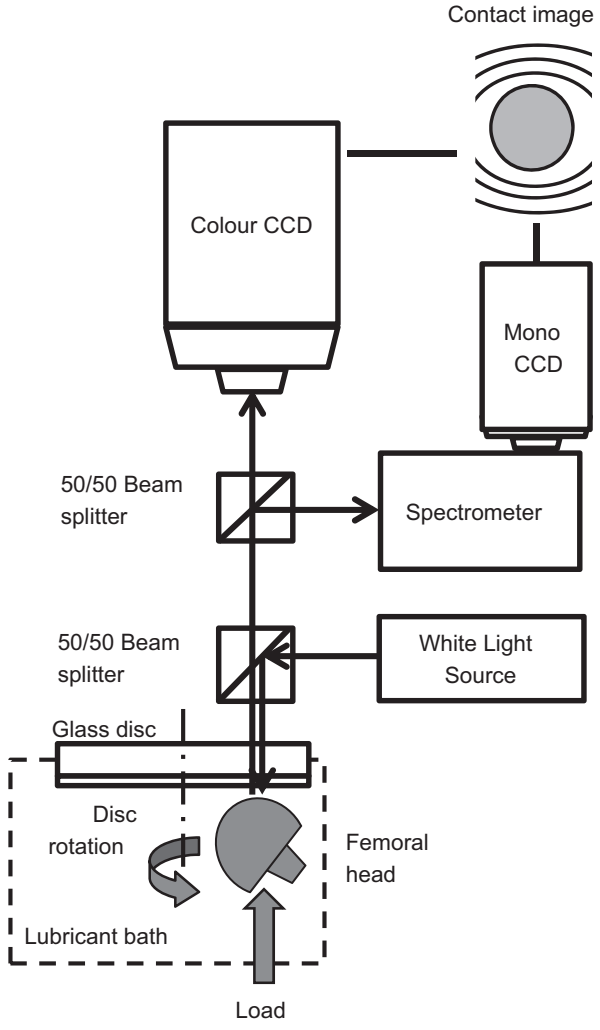

Fig. 4 – Schematic diagram of dual spectrometric and RGB optical interference image capture system, for film thickness measurements.

The ISO (2002) standard (#14242-1) which governs hip gait simulation for load and motion, defines hip articulation by a three axes coordinate system; flexion/extension (FE), adduction/abduction (AA) and inward/outward rotation (IOR), as shown in Fig. 1. The point of origin is considered the centre of the femoral head. The FE axis is assumed fixed at the pelvis and the AA axis floats, whilst the IOR axis is fixed through the femur (Reinisch et al., 2005). The IOR axis is also considered the loading axis. The angles of rotation around all three axes for a single gait cycle as defined by the ISO (2002) standard #14242-1 are shown in Fig. 2. During the gait cycle contact movement is only along the FE and AA planes. This forms a highly elliptical contact track which means that the contact is continuously sliding. By comparison a single axis reciprocating track would have zero speed at either end of the stroke. Fig. 3(a) shows the corresponding contact track for a 38 mm diameter femoral head, whilst Fig. 3(b) shows the compound speed and load for a single gait cycle. The contact track comprises of a high load and a low load side, these correspond to the 'stance phase' and 'swing phase', respectively (as shown in Fig. 3(a)). The stance phase begins with the 'heel strike' at $t=0$ and ends with the 'toe off' at $t=0.6$. Within the stance phase two loading peaks occur, the 'maximal weight acceptance' and 'push-off' points, respectively. Interestingly the second 'push-off' occurs at the minimum sliding speed, which represents the most destructive point in the gait cycle for lubricating film formation. In addition the IOR introduces a spin component throughout the gait cycle. As the IOR axis is fixed with the loading axis the origin of the spin can be assumed as the centre of the contact.

The ISO standard describes highly transient load and surface velocity conditions, where at no one point during the gait cycle can the contact be considered to be steady-state.

Such transient motion and loading will have negligible effects on film formation in a classical EHL model (Glovnea and Spikes, 2003). However as the PAL model is inlet-specific anything that disrupts the protein build-up and entrainment will affect the lubricant film thickness. It is therefore necessary to understand the effect of changing inlet condition and sliding direction on PAL. In addition the passage of surface defects or debris through the inlet would also be expected to have a significant effect on film formation beyond that occurring for EHL mechanisms.

2. Materials and methods

2.1. *Film thickness measurement and in-contact imaging*

Central film thickness measurements were made using a combined optical spectrometer and RGB analysis techniques (Ultra-Thin Film Measurement System, PCS Instruments, UK). This arrangement allowed visualisation of the inlet and contact region whilst simultaneously capturing spectrometer data of the central contact region. The dual measurement method allowed accurate film thickness measurements to be taken which give a true depiction of the entire contact film distribution. Optical interferometry is employed to take single position measurements within the central contact region, whilst the colour images provide a means of inferring film behaviour over the entire contact region. A schematic representation of the apparatus is shown in Fig. 4. Contact wear can also be estimated by monitoring the contact size in both image systems (Myant et al., 2012). The combined approach allows simultaneous measurement of film thickness and wear.

The contact was formed between a resurfacing CoCrMo femoral head (38 mm diameter) loaded against a coated glass disc. The underside of the glass disc was coated with a thin chromium layer (~10 nm) overlaid by silica (~500 nm). The head was held in a supporting mount and could be rotated so that a different position was used for each test. In all tests the femoral head was held stationary whilst the glass disc rotated, creating a pure sliding contact. Single-position film thickness measurements from the centre of the contact were obtained using the spectrometer. The technique measures central film thickness in the range 1–1000 nm with a resolution of ±1 nm. A PC controlled the temperature, load and sliding speeds.

The contact was lubricated with diluted 25% bovine calf serum (BCS Sigma Aldrich 12133C) and deionised water (Sigma Aldrich S-37531-356) solution, this corresponds to a protein concentration of *ca* 18 mg/L. The solutions were stored in a fridge (5 °C) immediately after preparation and used within 1 week; consequently it was not necessary to use antibacterial agents.

The test specimens were cleaned ultrasonically in 1% sodium dodecyl sulphonate solution in deionised water. The specimens were then rinsed three times in deionised water and finally washed in Analar isopropanol. Before the test specimens were air-dried and then mounted in the optical device, which was held at 37 °C for 1 h prior to testing. The sample pot was then filled with *ca* 200 mL of test fluid so that the underside of the disc and contact area was immersed in fluid.

2.2. *Inlet length: Definition and measurement*

Film thickness and distribution within the Hertzian contact region is a function of the lubricant supply immediately up stream of the contact (Wedeven, 1970); i.e. the rheological properties of the inlet reservoir. At first the contact is lubricated by the bulk phase, since the medium is continuous, these areas give very uniform interference fringes. However, due to PAL a new protein enriched phase is rapidly formed within the inlet region. This PAL phase can be identified by a shift in the location of the interference fringes. Fringes are shifted closer to the loaded region due to an increase in the refractive index and indicate a greater protein concentration. The inlet length reported in this paper refers to the length of the PAL inlet phase, taken from the edge of the Hertzian contact to the PAL inlet boundary. Fig. 5 shows a typical interference image of a sliding contact lubricated with 25% BCS, the PAL inlet phase is visible and has been clearly marked.

2.3. *Experimental programme*

To start, two tests were performed aimed at investigating film thickness dependency on the formation of the new inlet phase. For this both spectrometer and RGB video was captured of the contact during start-up motion. Then, once a stable film had formed, the contact was heavily disrupted by the passage of a large surface defect. A load of 2 N was maintained throughout the test period. A frame rate of 30 fps was employed for both monochromatic and RGB video capture. For the start-up case video was recorded of a static contact rapidly accelerated to a sliding speed of U_s=20 mm/s. The second test simulated the effect that debris and/or a surface defect would have on contact film thickness. For this videos were captured after constant sliding at U_s=20 mm/s for several minutes, so that a thick film had been formed. After which a scratch on the glass disc was allowed to pass through the contact. The scratch was several times larger than the contact width (*ca* 200 μm) and greater than 500 nm

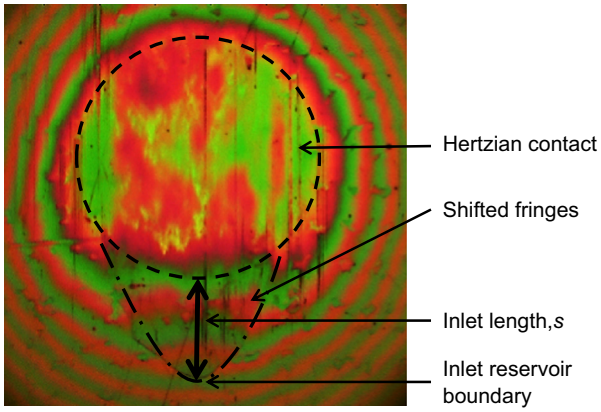

Fig. 5 – Typical interference image of a sliding contact lubricated with 25% BCS. The PAL inlet phase and inlet length are indicated.

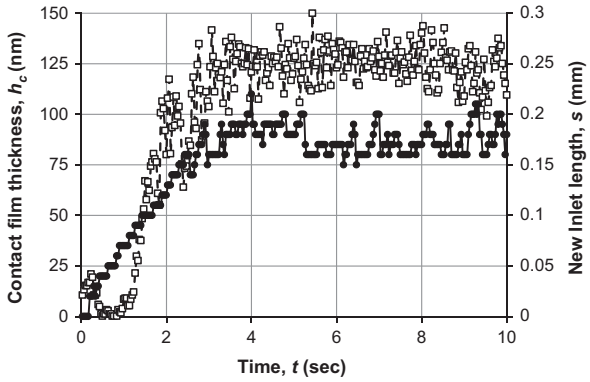

Fig. 6 – Contact film thickness (white squares) and inlet length (black triangles) *versus* time during start-up motion.

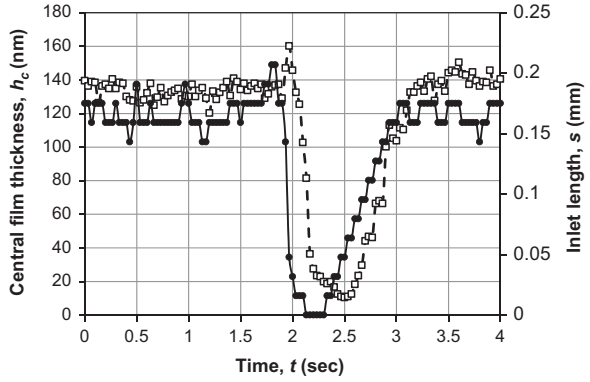

Fig. 7 – Film thickness (white squares) and Inlet length (black circles) plotted against time. The scratch passes through the contact at $t=1.8$ s.

in depth. The resulting film thickness and inlet size was determined.

To observe the effect of transient motion over a longer period of time, film thickness was measured for three types of motion. These were:

I. Constant speed (constant sliding direction); $U_s=20$ mm/s
II. Sinusoidal speed (constant sliding direction); $U_{s\_max}=20$ mm/s at 50% cycle, $U_{s\_min}=0$ at 0 and 100% cycle, $f=0.75$ Hz
III. Sinusoidal velocity (reversal in sliding direction over each cycle); $U_{s\_max}=\pm 20$ mm/s at 25 and 75% cycle, $U_{s\_min}=0$ at 0, 50 and 100% cycle, $f=0.75$ Hz

For each kinematic condition the tests were run for 1500 cycles. Film thickness was measured in two ways:

I. Sliding was stopped and the residual contact film captured at regular intervals over the test period. Image capture was conducted as quickly as possible before sliding continued; this process lasted no longer than a few seconds.
II. To determine contact film thickness during sliding, over an entire cycle, videos were captured for 4 cycles at the end of each test.

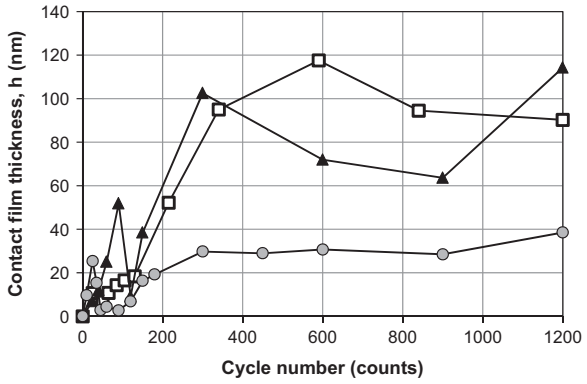

Fig. 8 – Optical interferometric film thickness measurements *versus* number of cycles for constant speed (white squares), sinusoidal speed (black triangles) and sinusoidal velocity (grey circles) cases.

3. Results

3.1. *Inlet dependency*

Fig. 6 shows a typical result during start-up motion; contact film thickness, h, and inlet length, s, are plotted against time. Time has been set to zero at the moment disc rotation is started; film thickness is 10 nm at $t=0$ s. Immediately after sliding begins an initial peak in film thickness of 20 nm is observed. After which, the film thickness decreases to zero before increasing again and stabilising at *ca* 125 nm, *ca* 2 s later. The inlet length can be seen to increase shortly after sliding has begun, increasing steadily for *ca* 2.5 s and plateauing at $s=0.175$ mm. There is a slight time offset between the increasing inlet length and film thickness of *ca* 0.25 s. After approximately 3 s the contact film thickness and inlet length stabilise. However, even in this 'steady-state' condition contact film thickness fluctuates by ± 20 nm, whilst inlet length varies continuously by up to 0.025 mm.

Fig. 7 shows a typical result for a steady-state condition when a surface defect passes through the contact. Film thickness, h, and inlet length, s, are plotted against time. Fluid was entrained into the contact for several minutes so that a 'steady-state' condition was formed. Then a deep scratch on the disc surface (formed transverse to the direction of motion) was allowed to pass through the contact. For the frame rate (30 fps), sliding speed (20 mm/s) and field of view (*ca* 0.5×0.35 mm) the scratch will pass through in a single frame. The scratch passes through at $\sim$1.7 s into the test. Until then film thickness and inlet length are relatively constant at 135 nm and 0.175 mm, respectively. Immediately after the scratch passes through the contact inlet length spikes, and then rapidly decreases to 0 mm over the next 0.3 s. A similar trend is observed for the contact film thickness; however, a time lag of $\sim$0.15 s exists. Once the inlet has been removed film thickness has decreased to 20 nm and slows. Film thickness reaches a minimum of 10 nm at 2.5 s. Film thickness and inlet length continue to increase over the next 0.5 s, until pre-scratch values are reached. At which point both film thickness and inlet length stabilise.

3.2. *Time dependent tests on transient motion*

This series of tests look at the effect transient motion has on lubricant behaviour and film formation. Figs. 8 and 9 show contact film thickness under constant speed (white squares), sinusoidal speed (black triangles) and sinusoidal velocity (grey circles). Fig. 8 shows the stationary residual film, whilst Fig. 9 presents real time film thickness values during each type of motion. Constant and sinusoidal speeds exhibit similar values; a final film thickness of *ca* 100 (±20) nm is achieved. In contrast the sinusoidal velocity case exhibits a significantly lower film thickness (*ca* 1/3) across the test period; a final film thickness of 25–30 nm is observed.

Fig. 9 presents the video captured film thickness data for 4 cycles for each entrainment speed case. For the constant speed test an average film thickness of 125 nm is maintained throughout the test period. For the sinusoidal speed case a similar average film thickness of 125 nm is achieved. A jump of *ca* 50 nm occurs shortly after the beginning of each cycle to reach a maximum cycle film thickness. Film thickness then decreases rapidly before increasing again at *ca* 50% cycle, when the maximum entrainment speed occurs. For the sinusoidal velocity case a significant reduction, of around 100 nm, in the overall film thickness is observed. In contrast to the sinusoidal speed case there are no sudden jumps in the film thickness after stationary ($U=0$) points in the cycle. Instead, maximum film thickness is observed at the beginning and end of each cycle and a minimum at 50% cycle.

4. Discussion

The results in Figs. 6–9 display non-classical lubricant behaviour; governed by protein-aggregation in the inlet. The films formed were much thicker than predicted by simple EHL models. These thick protein films helped protect the CoCrMo surface from wear (Myant et al., 2012). The relationship between inlet length and contact film thickness was clearly observed for all types of motion investigated. During steady-state, unidirectional, sliding the film thickness values oscillate widely (Fig. 6, $t>4$ s), this represents the chaotic nature of the film distribution across the contact and erratic inlet feed rate. It is worth noting here that, in contrast, according to classical EHL rules a simple, single phase, liquid experiencing the same steady state conditions would maintain a constant film thickness with no significant changes in film thickness (Sugimura and Spikes, 1996). Using Hooke's (1980) equations for isoviscous-EHL contacts the central film thickness, for a viscosity close to water ($\eta=0.001$ Pa s) is ~2 nm, at $W=2$ N and $U_s=20$ mm/s. This is significantly lower than the measured film thickness of *ca* 130 nm, observed for steady state sliding. If the viscosity is back calculated from the measured film thickness, the prediction is matched at $\eta=1.2$ Pa s. This is a rather crude method for calculating viscosity, and is dependent on which regression equations are employed. However, it does lend some further credence to the hypothesis that the new PAL inlet phase is exhibiting a much higher viscosity than the bulk phase.

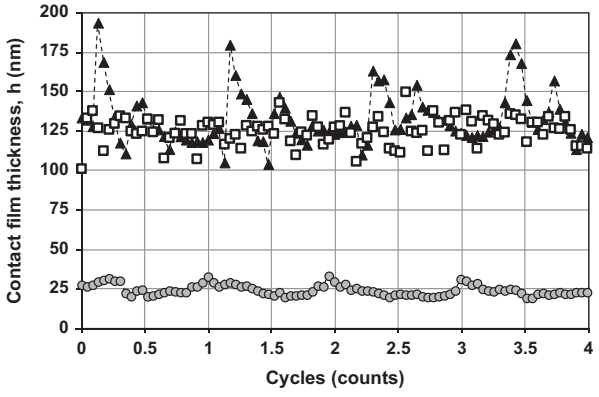

Fig. 9 – Optical interferometric film thickness measurements over four cycles for constant speed (white squares), sinusoidal speed (black triangle) and sinusoidal velocity (grey circles).

During start-up motion film thickness was observed to increase proportionally with inlet length. Fig. 10 presents the RGB interference images of the contact, captured at $t=0$, 1.7, 2.25, 2.5, 2.8 and 4 s during the inlet disruption test in Fig. 7. Lubricant flows from bottom to top in each image. Dark green represents areas of thinner films, whilst red represents areas of thicker films. The non-uniform film distribution within the contact can be seen in all images. The protein-rich phase is visible by discontinuities in the interference fringes within the inlet region. Through RGB image analysis it was observed that the thickest film was often present as a central strip through the contact, in the direction of sliding. This red strip can be seen to have a width and location which corresponds directly with the PAL inlet reservoir. Once the inlet is disrupted a significant reduction in film thickness occurs. RGB analysis, Fig. 10, reveals greater insights into lubricant behaviour. The scratch causes a sudden increase in inlet size, perhaps by pushing more proteins into it. As the scratch passes through the contact the surfaces are not 'stripped' as one might expect. Instead the inlet is disrupted in a manner which causes it to be sucked into the contact, thus causing a spike in film thickness. This process can be observed as the offset, in time, between *h* and *s* in Fig. 7; which indicates the time taken for proteins within the inlet to reach the contact centre. This speed is much slower than the surface speeds, suggesting the proteins do not freely pass through the main contact region. The inlet is completely removed by 0.3 s after the scratch has passed. At this point a thin film of 20 nm remains. No significant increase in inlet length occurs for a further 0.25 s. The contact is no longer 'fed' by the protein rich inlet reservoir; instead the remaining surface film decreases (worn away). By now the inlet has begun to recover, once again feeding the contact with the high viscosity phase. It is not clear if this is a result of a critical inlet length being achieved or simply an indication of how long the proteins take to travel from inlet to contact centre. It is clear that the PAL mechanism causes thick, protective, films to form within the contact; but once formed the films are extremely fragile and easily disrupted, or removed, by surface defects/debris or Inlet disruption. For the case presented in Fig. 7 the entire process of film removal and recovery takes just over 1 s.

Fig. 8 presents film thickness measurements taken shortly after halting of sliding motion. For a single phase Newtonian fluid, of a similar viscosity, the separating film rapidly decays

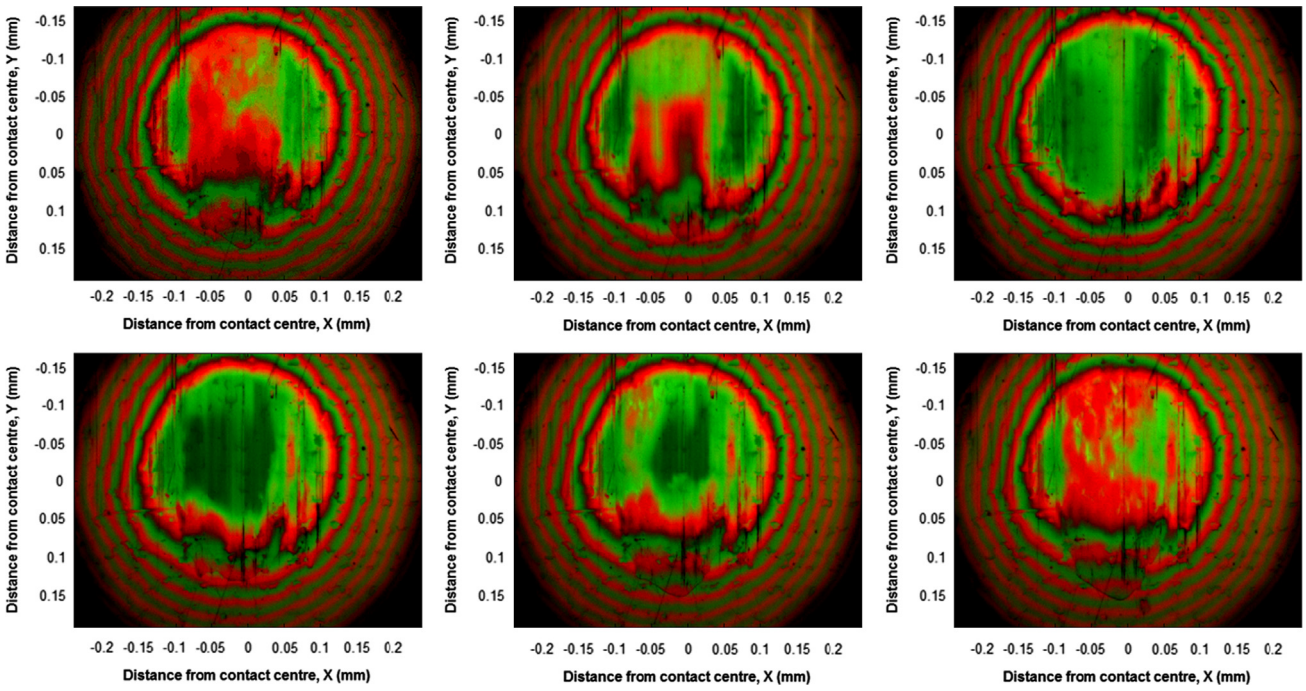

Fig. 10 – Colour interferometric images of the contact, captured at t=0, 1.7, 2.25, 2.5, 2.8 and 4 s during an inlet disruption test. Lubricant flows from bottom to top in each image. A 5 × magnification lens was employed for all images. (For interpretation of the references to color in this figure legend, the reader is referred to the web version of this article.)

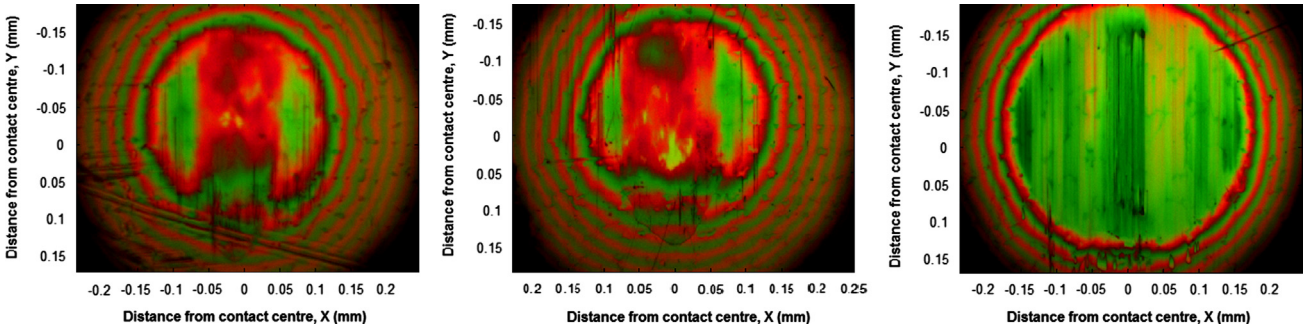

Fig. 11 – Colour interferometric images of the contact, captured at U_s=10 mm/s for constant speed (LHS), sinusoidal speed (Centre) and sinusoidal velocity (RHS). Lubricant flows from bottom to top in each image. A 5 × magnification lens was employed for all images. (For interpretation of the references to color in this figure legend, the reader is referred to the web version of this article.)

within the first second (Glovnea and Spikes, 2000). However, in this investigation thick films are recorded for all tests. This suggests that the thick protein films which build up under sliding have load bearing properties even after halting of motion. For uni-directional sliding a rapid increase in film thickness is observed over the first 300 cycles, film thickness then plateaus albeit with some scatter. A final film thickness of *ca* 100 (±20) nm is achieved. For the bi-directional tests films appear to be more 'stable' (less scatter). Similar, film thickness increases in the first 300 cycles and then plateauing at 25–30 nm for the remainder of the test.

Fig. 9 shows some interesting results on the difference between sinusoidal uni-directional and sinusoidal bi-directional sliding. In disagreement with classical EHL rules the maximum film thickness does not occur at the maximum speed for both cases. For sinusoidal uni-directional sliding a large jump in film thickness occurs shortly after sliding begins. This is caused by a sudden intake of inlet aggregates (observed through RGB image analysis). It might be that at zero speed proteins and other molecules present within the inlet reservoir have increased surface interaction which results in greater surface drag forces (into the contact) at the start of each cycle/sliding. In contrast, the sinusoidal velocity case, there are no sudden jumps in the film thickness after stationary points in the cycle. The maximum film thickness is observed at the beginning and end of each cycle and a minimum at 50% cycle. This is rather surprising as entrainment speed is zero at all three points (Fig. 8). One might have expected a simple doubling in the frequency of the sinusoidal speed case; peaks immediately after each

stationary point of the cycle. It is worth noting that for a simple, Newtonian, fluid two film thickness peaks corresponding to the maximum entrainment speeds at 25 and 75% cycle would be observed (Glovnea and Spikes, 2002). Instead, it appears as though the film is exhibiting directional memory. Film thickness increases and decreases with a change in the sliding sign, causing an asymmetric film/velocity profile. The positive direction dependent on the initial sliding direction, however it is likely that this will even out over time. A more in-depth study is currently being carried out regarding the intricacies of this behaviour. It is clear that a change in the direction of lubricant flow disrupts the formation of the protein film.

Fig. 11 shows three colour interference images of the contact at U_s=20 mm/s. The images show the contact during the last few cycles of each test. By measuring the contact size at the beginning and end of the test it is possible to estimate the wear. A small increase in contact radius of *ca* 3% was observed for the uni-directional sliding tests, whereas an increase of >60% is seen for the sinusoidal velocity (bi-directional) case. As reported in earlier papers (Myant et al., 2012) the formation of thick contact films protects the CoCrMo surface from aggressive wear. Fig. 11 demonstrates the subsequent high wear rate caused by continual disruption of this protective film. The protein rich inlet reservoir is clearly visible for the constant and sinusoidal speed cases, whilst its absence is obvious for the sinusoidal velocity test. It is clear that the formation of thick, protective, contact films is only possible with the presence of the high viscosity inlet phase.

4.1. *Implications for hip implant lubrication*

The PAL mechanism is determined by the viscous material present in the inlet, which is why a reversal in sliding direction has such a significant effect on film formation. Similarly the results have demonstrated that the passage of scratches and debris can also displace this material. The protective film is stripped exposing the CoCrMo to tribo-corrosive mechanisms and accelerating wear. Compared to EHL mechanisms where film recovery is almost instantaneous (Jalali-Vahid et al., 2006), the measured film was observed to build more slowly as the viscous reservoir was replenished. During this period there is an increased risk of wear. Poorly aligned components will promote edge loading and increased contact pressures (Underwood et al., 2012); our results indicate these films are very sensitive to increased pressures (Myant et al., 2012). Edge loaded contacts may mimic scratch-like behaviour, completely stripping the surface film and accelerating wear. Carbide precipitates have been reported for numerous CoCrMo alloys which break off the surface, creating a surface defect and forming debris. It is likely that debris will have the same detrimental effect on film thickness as a surface scratch.

In this investigation uni-directional and bi-directional single axis sliding was investigated. For the uni-directional tests there is no significant disruption in the inlet region, unless an artefact (scratch etc.) passes through the contact. For the bi-directional case the inlet is heavily disrupted in every cycle, significantly inhibiting the build-up of a protein rich inlet phase. Fig. 3 shows that, for the ISO standard, the contact track is ellipsoidal (two axes); not a single axis reciprocating stroke as tested in this paper. It is, therefore, likely that inlet disruption is not as severe as the bi-directional case tested. However, the IOR was not included in this investigation due to limitation in the test rig. The IOR introduces spin. Spin has been well studied for point (Li et al., 2010) and elliptical (Dowson et al., 1993; Zou et al., 1999) bearing contacts. The spin will introduce additional off-axis flow forces in the direction of spin rotation within the inlet region; further disrupting the PAL mechanism. Within the main contact zone, spin will hinder and/or aid entrainment of fluid, either side of the central flow line (Li et al., 2010). However, the effect of spin has not been investigated for complex fluids and caution must be taken when applying previous studies to SF lubricated articular joints.

The PAL mechanism also has implications for the design of screening tests as it is an Inlet specific lubrication mechanism. Simple screening tests, such as pin-on-disc tribometers which employ continuous uni-directional sliding, may observe low wear rates compared to explant studies. It is also important to note that transient speeds had little effect on the average film thickness, which implies 'cross shear' tests may also be at risk of low wear rates as they do not disrupt the inlet flow enough. Reversal in sliding direction is, perhaps, the most important parameter to simulate when investigating bearing performance during articular motion.

5. Conclusions

This investigation has explored lubricant behaviour and film formation mechanisms under transient conditions. Further evidence for a novel film formation mechanism has been presented. Our conclusions are as follows:

(1) BCS lubrication behaviour is dominated by the formation of protein-rich, high-viscosity phase of aggregated molecules at the inlet to the contact zone.
(2) The viscous material is entrained into the contact forming much thicker films than predicted by classical EHL models for simple fluids.
(3) The high-viscosity material continues to separate the surfaces even under stationary-loaded conditions; this could provide protection of surfaces at start-up or at stance.
(4) Film formation is very susceptible to disruption of the inlet reservoir; this could be due to changes in the direction of sliding motion, entrained debris or surface scratches.
(5) The PAL mechanism has significant implications for the development of pertinent screening tests and appropriate test fluids. Reversal in sliding direction is, perhaps, the most important parameter to simulate when investigating bearing performance during articular motion.
(6) MoM hip implants with increased risk of edge loading are likely to have cyclic removal of the protective protein layer. Subjecting it to accelerated wear conditions.

Acknowledgements

The authors wish to thank the UK EPSRC for funding this research: "In Contact Analysis of Synovial Fluid Lubricating Film Properties" (EP/H020837/1) and Platform Grant

"Nanotribology: Measurement and Modelling across the Rubbing Interface" (EP/G026114/1).

REFERENCES

Dowson, D., Neville, A., 2006. Bio-tribology and bio-mimetics in the operating environment. Proc. Inst. Mech. Eng. Part J J. Eng. Tribol. 220, 109–123.

Dowson, D., et al., 1993. Elastohvdrodvnamic lubrication of elliptical contacts with pure spin. Proc. Inst. Mech. Eng. Part C J. Mech. Eng. Sci. 207, 83–92.

Fan, J., et al., 2011. Inlet protein aggregation: a new mechanism for lubricating film formation with model synovial fluids. Proc. Inst. Mech. Eng. Part H J. Eng. Med. 25, 696–709.

Glovnea, R.P., Spikes, H.A., 2000. The influence of lubricant upon EHD film behavior during sudden halting of motion. Tribol. Trans. 43, 731–739.

Glovnea, R.P., Spikes, H.A., 2002. Behavior of EHD films during reversal of entrainment in cyclically accelerated/decelerated motion. Tribol. Trans. 45, 177–184.

Glovnea, R.P., Spikes, H.A., 2003. Oscillation induced in EHD film thickness by a step in entrainment speed. Lubr. Sci. 15, 311 (230).

Hamrock, B.J., Dowson, D., 1978. Elastohydrodynamic lubrication of elliptical contacts for materials of low elastic modulus: 1. Fully flooded conjunction. J. Lubric. Technol. Trans. ASME 100, 236–245.

Hooke, C.J., 1980. The elastohydrodynamic lubrication of heavily-loaded point contacts. J. Mech. Eng. Sci. 22, 183–187.

ISO 14242-1, 2002. Implants for Surgery – Wear of Total Hip-joint Prostheses – Part 1: Loading and Displacement Parameters for Wear-testing Machines and Corresponding Environmental Conditions for Test.

Jalali-Vahid, D., et al., 2006. Effect of start-up conditions on elastohydrodynamics lubrication of metal-on-metal hip implants. Proc. Inst. Mech. Eng. Part H J. Eng. Med. 220, 143–150.

Li, X.M., et al., 2010. Influence of spinning on the rolling EHL films. Tribol. Int. 43, 2020–2028.

Myant, C., Cann, P., 2013. In contact observation of model synovial fluid lubricating mechanisms. Tribol. Int. 63, 97–104.

Myant, C., Cann, P., 2014. On the matter of synovial fluid lubrication: implications for metal-on-metal hip tribology. J. Mech. Behav. Biomed. Mater. ⟨http://dx.doi.org/10.1016/j.jmbbm.2013.12.016⟩.

Myant, C., et al., 2012. Lubrication of metal-on-metal hip joints: the effect of protein content and load on film formation and wear. J. Mech. Behav. Biomed. Mater. 6, 30–40.

Reinisch, G., et al., 2005. Differences of the mechanical setup of hip simulators and their consequences on the outcome of hip wear testing. J. ASTM Int. 3, 1–15.

Smith, S.L., Dowson, D., Goldsmith, A.A.J., 2001. The lubrication of metal-on-metal total hip joints: a slide down the Stribeck curve. Proc. Inst. Mech. Eng. Part E J. Process Mech. Eng. 215, 483–493.

Stachowiak, G.W., Batchelor, A.W., 2005. Engineering Tribology. Elsevier Butterworth-Heinemann, Oxford, UK.

Stokes, J.R., Wolf, B., Frith, W.J., 2001. Phase-separated biopolymer mixture rheology: prediction using a viscoelastic emulsion model. J. Rheol. 45, 1173–1191.

Sugimura, J., Spikes, H.A., 1996. Technique for measuring EHD film thickness in non-steady state contact conditions. In: Dowson D. et al. (Eds.), Proceedings of the 23rd Leeds–Lyon Symposium on Tribology. Elastohydrodynamics.

Underwood, R.J., et al., 2012. Edge loading in metal-on-metal hips: low clearance is a new risk factor. Proc. Inst. Mech. Eng. Part H J. Eng. Med. 226, 217–226.

Wedeven, L.D., 1970. Optical Measurements in Elastohydrodynamic Rolling Contact Bearings. Ph.D. Thesis. Imperial College Press.

Yew, A., et al., 2004. Analysis of elastohydrodynamic lubrication in McKee–Farrar metal-on-metal hip joint replacement. Proc. Inst. Mech. Eng. Part H J. Eng. Med. 218, 27–34.

Zou, Q., et al., 1999. Elastohydrodynamic film thickness in elliptical contacts with spinning and rolling. Trans. ASME 121, 686–692.